Journal of Materials Science: Materials in Electronics (2018) 29:17234–17244
https://doi.org/10.1007/s10854-018-9817-2

Growth of cobalt–nickel layered double hydroxide on nitrogen-doped graphene by simple co-precipitation method for supercapacitor electrodes

Hui Xu[1] · Junxia Wu[1,2] · Jian Liu[1] · Yong Chen[1] · Xin Fan[1]

Received: 13 January 2018 / Accepted: 3 August 2018 / Published online: 28 August 2018

Abstract
Nitrogen-doped graphene/Co–Ni layered double hydroxide (RGN/Co–Ni LDH) is synthesized by a facile co-precipitation method. Transmission electron microscopy images indicated that the formation of Co–Ni$(OH)_2$ nanoflakes with the good dispersion anchored on the surfaces of the nitrogen-doped graphene sheets. The nitrogen-doped graphene composites delivered the enhanced electrochemical performances compared to the pure Co–Ni LDH due to the improved electronic conductivity and its hierarchical layer structures. The high specific capacitance of 2092 F g^{-1} at current density of 5 mA cm^{-2} and the rate retention of 86.5% at current density of 5–50 mA cm^{-2} are achieved by RGN/Co–Ni LDH, higher than that of pure Co–Ni LDH (1479 F g^{-1} and 76.5%). Moreover, the two-electrode asymmetric supercapacitor, with the RGN/Co–Ni LDH composites as the positive electrode and active carbon as the negative electrode material, exhibits energy density of 49.4 Wh kg^{-1} and power density of 101.97 W kg^{-1} at the current density of 5 mA cm^{-2}, indicating the composite has better capacitive behavior.

1 Introduction

In recent years, with the continuous reducing of fossil energy and the aggravation of environmental pollution, looking for efficient as well as green energy storage equipment is imminent. Supercapacitors, which are also called electrochemical capacitors have received great attention all over the world because of their superior power density and higher energy density compared to batteries and conventional capacitors, respectively [1]. According to the energy storage mechanism, supercapacitors are classified into two types, including electrical double-layer capacitors (EDLC) and pseudocapacitors. EDLC arises from the accumulated charge on the interface between electrode and electrolyte. The pseudocapacitors occurred fast and reversible faradic reactions during the charge/discharge process [2]. So as far, different materials have been researched in order to obtain supercapacitors with excellent electrochemical performances, including carbons, transition metal oxide/hydroxides and conducting polymers [3]. Currently, the carbon-based materials with good cycle lifetime and higher power density mainly served as the electrode of EDLC. Among all kinds of carbon materials, graphene has been considered as an ideal candidate for electrode materials on account of its outstanding electrical properties, excellent mechanical strength, ultrahigh specific area and reasonable thermal conductivity [4]. In recent years, the numerious applications of graphene-based materials in supercapacitors have been carried out by researchers. Due to Van der Waals interaction, graphene nanosheets often suffer from serious agglomeration or re-stacking, which hinder wider application of graphene based supercapacitors. So, improvements in their electronic, chemical and structural properties of the graphene in the nanometer scale remain a key task for practical applications [5]. Recently, nitrogen-doped graphene have aroused great attention because introduction of N into graphene during the reduction process may improve the electrochemically performance of graphene. Nitrogen atoms have similar sizes and valence electron numbers as carbon, hence it is easier to incorporate into graphene and cause extra n-type carriers in carbon systems, which are ascribed to the conjugation between the nitrogen lone-pair electrons

✉ Hui Xu
xuhui@lut.cn

[1] College of Petrochemical Technology, Lanzhou University of Technology, Lanzhou 730050, China

[2] Baiyin Institute of Mining and Metallurgy, Baiyin 730900, China

and the grapheme π system [6]. Nitrogen doped graphene can not only improve specific capacitors of graphene materials, but also reduce the bundling and restacking of graphene layers to increase specific surface area and active sites of graphene [7]. To date, many nitrogen doped graphene have been synthesized by various methods and investigated for the energy storages [8–10]. However as one of carbon materials, in terms of EDLC's charge-storage mechanism, low specific capacitance and energy density confine their practical applications as electrode materials [11]. On the contrary, pseudocapacitors can obtain much higher specific capacitance and energy density than traditional EDLCs due to reversible redox faradaic reactions. Until now, pseudocapacitive materials such as transition metal oxide/hydroxide, conducting polymers, as well as their composites with carbon matrix have been employed for the application in pseudocapacitors [12–14]. Among various materials used for pseudocapacitors, layered double hydroxides (LDHs) have been greatly concerned in supercapacitors due to their high enough specific capacitance and energy density. LDHs with abundant slabs structure are usually expressed by formula $[M^{2+}_{(1-X)}M^{3+}_{(X)}(OH)_2]^{X+}(A^{n-})_{X/n}{\cdot}mH_2O$, where M^{2+} and M^{3+} represents the divalent and trivalent metallic cation (such as Ca^{2+}, Mg^{2+}, Co^{2+}, Al^{3+}, Fe^{3+}, etc.) and A^{n-} is an interlayer anion. The water molecules were embedded in the interlayer structure [15]. Many investigations have been performed to synthesize LDHs which containing Ni, Co, Al, Mn, Cu etc. and measure their electrochemical performances. Pan et al. [16] prepared Co–Al layered double hydroxide, it exhibited a high specific capacitance of 930 F g^{-1} at 2 A g^{-1}. Wang et al. [17] reported Ni–Al LDH coated on nickel foam as high performance supercapacitors, which could display the specific capacitance of 701 F g^{-1} at a current density of 10 mA cm^{-2}. In particular cobalt–nickle layered double hydroxide (Co–Ni LDH) is one of the most promising electrode materials because of its high theoretical-capacitance value of > 3000 F g^{-1} and superior redox activity [18]. However, the pseudocapacitors applications of LDH are limited due to their poor electrical conductivity and agglomeration effect, which hinder their charge/discharge rate, as well as the power performance of LDH as high-power electrode materials [19]. To overcome these drawbacks, LDH is used to combine with conductive carbon materials such as carbon nanotubes, activated carbon and graphene to form a composite [20]. Carbon materials, in particular graphene, can provide large surface areas and high conductivity to prevent LDHs from agglomeration, facilitate electrical conductivity and enhance mechanical stability. To utilize the advantages of two kinds of materials, many these graphene/LDHs hybrids have been designed and exhibited outstanding capacitance and rate performance, indicating their promising potential as electrode materials for the application in high-performance supercapacitors. For instances, Milan et al. [21] prepared Ni–Co binary hydroxide on a reduced graphene oxide directing template over nickel foam substrate. The composite exhibits a high specific capacitance of 2130 F g^{-1} at 2 A g^{-1} and well cycles stability. Patil et al. [22] described a two steps method to develop Co–Ni hydroxides over 3D graphene foam, it exhibits a maximum specific capacitance of 1847 F g^{-1} at a discharge current density of 5 A g^{-1}. Tiruneh et al. [23] reported Lamellar Co–Ni$(OH)_2$/rGO structures were prepared by co-precipitation followed by hydrothermal synthesis. The composite displays a specific capacitance of 811 F g^{-1} at 0.5 A g^{-1} with the highest capacitance retention of 90% at 2 A g^{-1} and good cycling stability. Among the reported CoNi-LDH hybrids, the graphene components were from the precursors of graphite oxide or other carbon sources without introduction of heteroatom N. However, nitrogen doping graphene as grown substrate for CoNi-LDH is rarely reported up to now.

In this work, we aimed to synthesize pure Co–Ni LDH, nitrogen-doped reduced graphene oxide (RGN) and Co–Ni LDH composite by simple co-precipitation method. The nitrogen-doped graphene were prepared in advance by hydrothermal precess. In the composites, LDH nanosheets are anchored onto the surfaces of RGN substrate to form a hierarchical architecture. Electrochemical measurements show that RGN/Co–Ni LDH composite exhibits high specific capacitance (2092.3 F g^{-1} at 5 mA cm^{-2}), fair rate capability and long cycling life. In addition, an asymmetric capacitor is designed with RGN/Co–Ni LDH and activated carbon (AC) as positive and negative materials, respectively.

2 Experimental section

2.1 Materials

Graphite powder(800 mesh) was purchased from Qingdao Henglide Graphite Co., Ltd., China. Urea, potassium permanganatepre, hydrogen peroxide (30% H_2O_2), nickel chloride hexahydrate and cobalt chloride hexahydrate ($CoCl_2{\cdot}6H_2O$) were obtained from Tianjin Damao Chemical Reagent Factory, China. All other reagents and solvents were obtained from commercial suppliers. All aqueous solutions were prepared with deionized water.

2.2 Preparation of materials

2.2.1 Preparation of nitrogen-doped graphene (RGN)

Nitrogen-doped graphene (RGN) was synthesised in our former work [24]. Graphite oxide (GO) was prepared by modified Hummer's method. 60 mg of GO was dispersed in 30 mL deionized water under sonication for 1 h to form homogeneous solution (2 mg mL^{-1}). Then, 0.6 g of urea

was added into the GO dispersion with further sonication for 2 h. The mixtures were transferred into a 50 mL Teflon-lined stainless-steel autoclave, and treated hydrothermally at 160 °C for 5 h. Afterwards, the autoclave was naturally cooled to room temperature and the hydrogel material of RGN was obtained. The product was washed with alcohol and deionized water for several times and freeze-dried in a vacuum oven for 12 h.

2.2.2 Preparation of RGN/Co–Ni LDH composites

An amount of RGN and 0.08 mmol of CTAB were added to 20 mL of deionized water and sonication for 2 h to form a uniform RGN solution. 1.1642 g of $CoCl_2{\cdot}6H_2O$ and 1.4266 g of $NiCl_2{\cdot}6H_2O$ were added to 70 mL of deionized water and stirring for 1 h. Then RGN solution were added to the formed solution and stirring for 1 h. Then ammonia solution was dropwise added to adjust pH to 9–10. Afterwards, the mixture was stirring for 3 h at room temperature. The RGN/Co–Ni LDH was obtained by filtered and washed in deionized water and finally dried under vacuum at 60 °C for 12 h.

For a comparative study, pure Co–Ni LDH was fabricated following the process as preparing RGN/CoNi-LDH without adding RGN solution.

2.3 Materials characterization

The phase structure of the samples were analyzed by XRD patterns obtained by D/MAX-2400X X-ray diffractometer with Cu Kα radiation (λ = 0.154056 nm). Fourier transformed infrared spectroscopy (FT-IR, Thermo Nicolet 6700) were recorded in the range 400–4000 cm^{-1}. The morphology of the samples were observed by field emission scanning electron microscope (SEM, JEOL JSM-6701F) and transmission electron microscope (TEM, JEM-1200EX, JEOL). X-ray photoelectron spectroscopy (XPS, PHI 5702). Raman spectra were obtained on a Renishaw RM2000 Raman spectrometer.

2.4 Preparation of electrode material and electrochemical measurements

The working electrode was prepared as follows. The cathode was prepared by mixing the electroactive material (75 wt%), carbon black (10 wt%), acetylene black (10 wt%) and polytetrafluoroethylene (5 wt%) in ethanol solvent. Then, the resulting slurry was coated onto the nickel foam substrate (1 cm × 1 cm) and dried at 80 °C under vacuum for 12 h. Finally, the electrode was pressed under a pressure of 15 Mpa. The mass of electroactive material in each electrode is approximately 6.5 mg.

The electrochemical measurements were measured by a three-electrode system, in which platinum electrode, saturated calomel electrode (SCE) and active material were used as counter electrode, reference electrode and work electrode, respectively. 6 M KOH aqueous was acted as electrolyte solution. The cycle voltammetry (CV) tests were performed between − 0.2 and 0.6 V (vs. SCE) at different scan rates. Galvanostatic charge and discharge (GCD) test was carried out in potential windows from − 0.1 to 0.35 V (vs. SCE) at different current densities. Electrochemical impedance spectroscopy (EIS) measurements were measured at a frequency range from 0.01 to 10^5 Hz with potential amplitude of 5 mV. The specific capacitance, energy density [E (Wh Kg^{-1})] and power density [P (W Kg^{-1})] of the samples was calculated according to the equation [24]:

$$C_s = I\Delta t/m\Delta V \tag{1}$$

$$E = C(\Delta V)^2/2 \tag{2}$$

$$P = E/\Delta t \tag{3}$$

where m is the mass of active material, and I, Δt, ΔV, C_s, E, P are the discharge current, total discharge time, potential drop during discharge, specific capacitance, energy density and power density, respectively.

3 Results and discussion

3.1 Morphology and structure characterization

The morphology and structure of RGN, Co–Ni LDH and RGN/Co–Ni LDH were revealed by SEM and TEM image analysis. Typical SEM image of the freeze-dried porous RGN is shown in Fig. 1a, it can be seen that RGN has a layered and porous three dimensional structure, which is attributed to the partially GO nanosheets was coalesced, strong cross-links of three-dimensional graphene network were formed with the assistance of Van der Waals' forces, π–π stacking and abundant hydrogen bonds of water during the hydrothermal process [25]. Figure 1b shows Co–Ni LDH particles with a regular little diameter of about 20 nm were tightly agglomerated together, resulting in poor contact area with the electrolyte. Figure 1c shows that the Co–Ni LDH petals were vertically grown over RGN surface to form 3D flower-like structure. During the co-precipitation process, cobalt and nickel ions were absorbed on the surface of RGN nanosheets by electrostatic adherence, followed by the nucleation and growth of the Co–Ni LDH crystallites. Besides, RGN could support Co–Ni LDH as a substrate, which can improve the agglomeration of Co–Ni LDH. The stacking of Co–Ni LDH is effectively prevented by the heterogeneous structure. Such hierarchical layer structures of

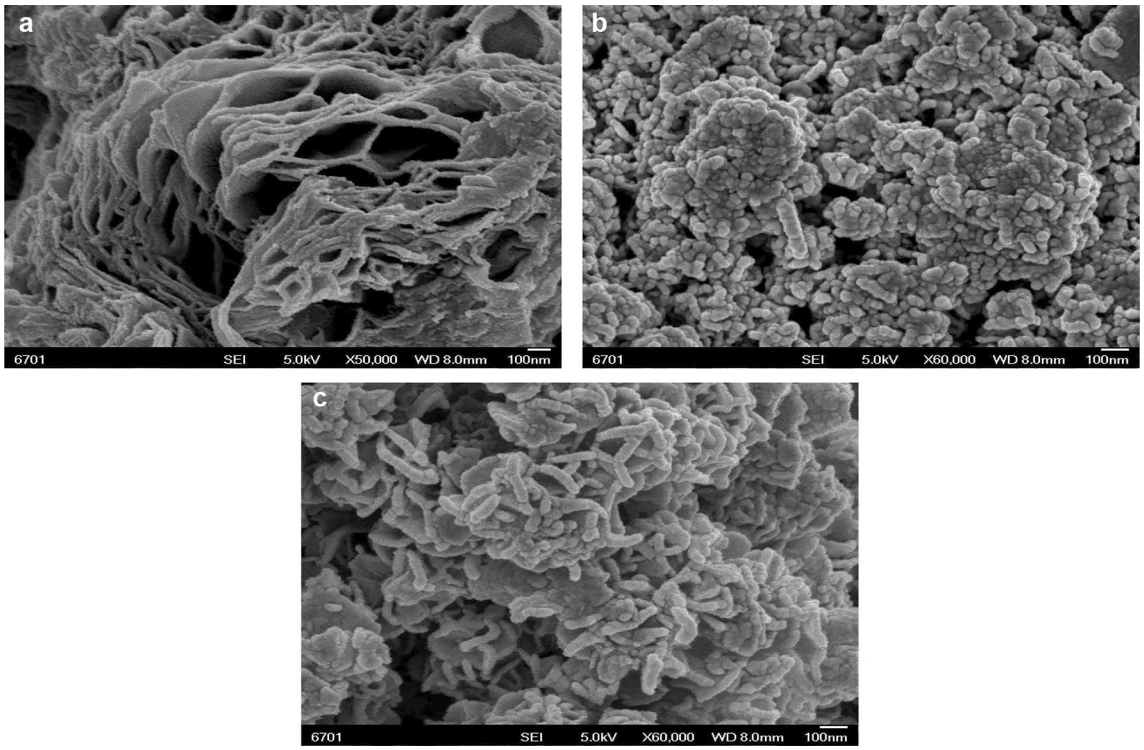

Fig. 1 SEM images of **a** RGN; **b** CoNi-LDH; **c** RGN/CoNi-LDH

RGN/Co–Ni LDH composite can increase the contact area between electroactive sites and electrolyte for promoting electrode reactions [26].

The SEM images of RGN, Co–Ni LDH and RGN/Co–Ni LDH are shown in Fig. 2. Figure 2a shows the typical TEM images of RGN, it has a voile-like structure and graphene planar surface with more corrugations and scrolling than the pristine graphene, indicating nitrogen atom was doped [27]. Figure 2b reveals the morphology of pure Co–Ni LDH, pure Co–Ni LDH nanosheets are laminated and slit-shaped agglomerated, displaying flower-like morphology. TEM image in Fig. 2c indicates that the surface of RGN are fully covered with Co–Ni LDH nanosheets. RGN nanosheets provide a scaffold-like structure and large contact area with the electrolyte for electron and ion transfer during the electrochemical process, in addition, it can prevent the agglomeration of CoNi-LDH effectively. The selected area electron diffraction (SAED) pattern of the RGN/CoNi-LDH shows clear multiple diffraction rings, caused by the growth of LDH on the surfaces of RGN and confirms the polycrystalline nature of of CoNi-LDH composite [28].

The surface functional groups of the corresponding samples are examined by FT-IR spectra. The FT-IR spectra of GO, RGN, CoNi FT-IR LDH and RGN/CoNi FT-IR LDH hybrids are shown in Fig. 3. Figure 3 shows that there is wide OH band at around 3400 cm in all the samples, which come from the O–H stretching vibrations of water molecules. For GO, weak absorption bands around 1730 and 1224 cm^{-1} are corresponding to the vibration of C=O and C–O functional groups. The strong absorption bands around 1630 cm^{-1} are C=C stretching vibrations [29]. For RGN, C=C stretching vibrations shift its wavenumber from 1630 to 1570 cm^{-1} due to doping nitrogen atom, C–H at 1396 cm^{-1} [30]. What's more, the new bands at 3137 cm^{-1} assigned to the N–H stretching vibrations. Moreover, the adsorption bands of oxygen-containing functional group (C=O, C–O) on RGN disappeared owing to the deoxygenation towards GO by urea and hydrothermal process. For CoNi-LDH and RGN/CoNi-LDH, the bands at 3440 cm^{-1} and 1629 cm^{-1} come from the O–H stretching vibrations of water molecules and the hydrogen bonding among the hydroxyl groups in all LDH samples [31]. The bands at 1394 cm^{-1} in pure CoNi-LDH and the hybrids are attributed to the vibration of CO_3^{2-} anion in the interlayer space [32]. These bands below 800 cm^{-1} come from the stretching and bending vibrations of metal–oxygen (M–O) in the hydrotalcite-like lattice [33]. For RGN/CoNi-LDH, the only difference between CoNi-LDH and RGN/CoNi-LDH is the band at 1484 cm^{-1} coming from bending vibration of RGN, indicating the co-existence of CoNi-LDH and RGN in the product.

XRD is conducted to characterize the phase structures. Figure 4a shows the XRD patterns of GO and RGN. The acute diffraction peak at $2\theta = 10.8°$ is ascribed to the (001) plane of GO for the GO pattern [34]. The completely

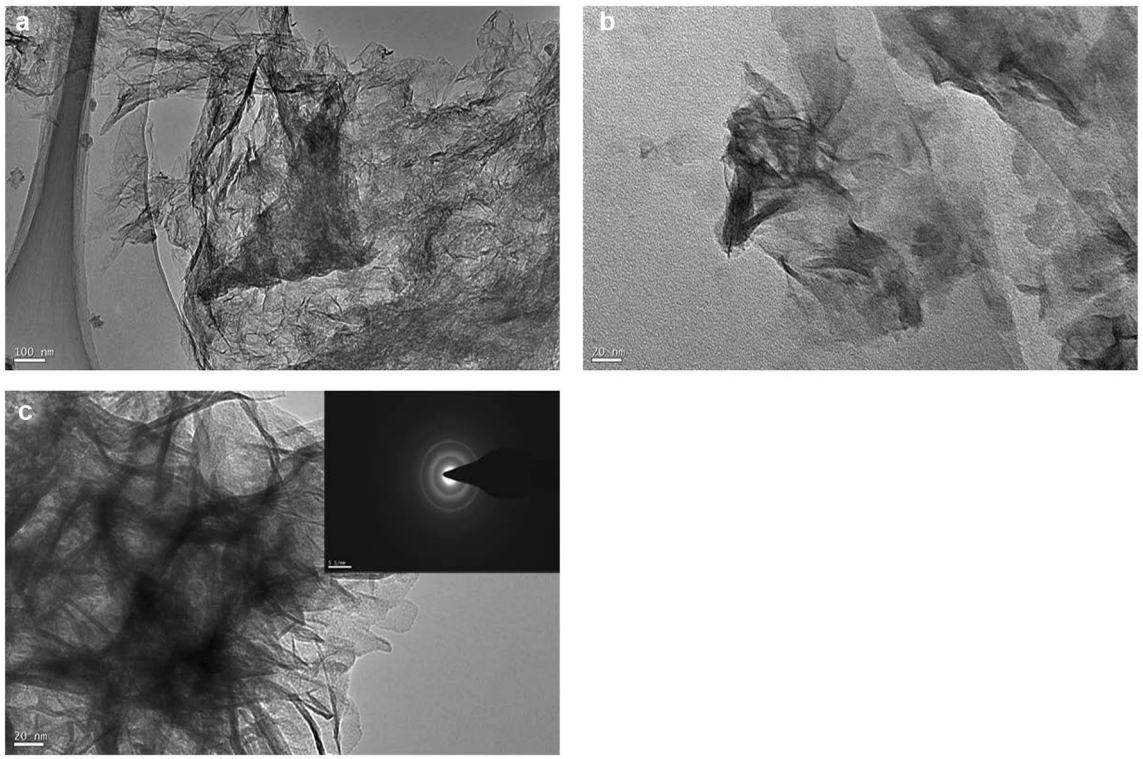

Fig. 2 TEM images of **a** RGN, **b** SAED pattern of CoNi-LDH, **c** SAED pattern of RGN/CoNi-LDH

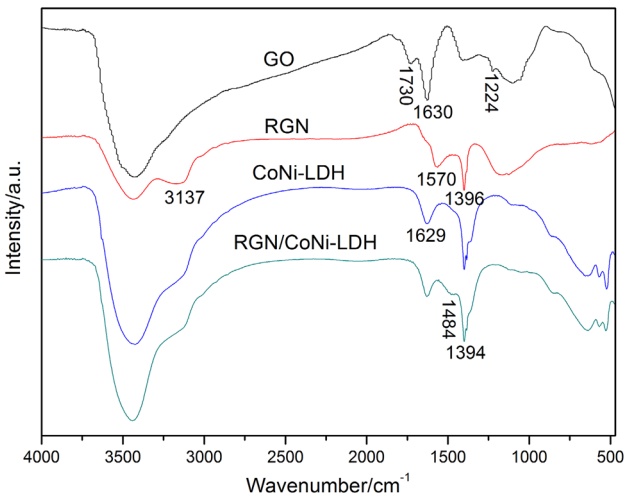

Fig. 3 FT-IR spectra of GO, RGN, CoNi-LDH and RGN/CoNi-LDH

disappearance of the (001) peak and the appearance of a new peak (002) at 2θ = 22° of RGN illustrate that graphite oxide was reduced by the urea after the hydrothermal reaction. The broad diffraction peak of RGN reveals that interlayer spacing of graphite nanosheets is widened by the exfoliation and reduced of GO in the hybrids. Figure 4b shows the XRD patterns of CoNi-LDH and RGN/CoNi-LDH. It can be seen from the curve of CoNi-LDH that the five diffraction peaks at 2θ values of 11.1° (003), 22.1° (006), 34.4° (009), 38.6° (015) and 60.7° (110) which can be corresponded to the planes of hydrotalcite-like LDH phase (JCPDS: 38-0487) [35]. The peak values of CoNi-LDH can also be observed in the curve of RGN/CoNi-LDH composite, revealing the existence of CoNi-LDH in the RGN/CoNi-LDH composite. However, the peak at 2θ = 22° in the RGN/CoNi-LDH is broader than CoNi-LDH, which is attributed to 2θ = 22° of RGN overlaps 2θ = 22.1° (006) of CoNi-LDH.

Raman spectroscopy is a well technique used to research the order/disordered crystal structure of materials. The presence of RGN in the composites was further proved using Raman spectroscopy. Figure 5 shows the Raman spectra of the RGN, CoNi-LDH and RGN/CoNi-LDH. The spectrum of the RGN displays two dominant D bands and G bands at 1352 cm^{-1} and 1589 cm^{-1}, respectively. The G band is related to the vibration of sp^2 carbon, while the D band is associated with the disorder degree in the graphene layers [36]. Furthermore, the intensity ratio of D band to G band (I_D/I_G) is used to estimate the disorder degree of carbon material. CoNi-LDH composite show two peaks at 468.46 and 528.78 cm^{-1}, which correspond to Ni–O and Co–O vibrational modes, respectively [37]. RGN/CoNi-LDH composite not only exhibit the peaks of CoNi-LDH composite, but also possess D bands and G bands of RGN.

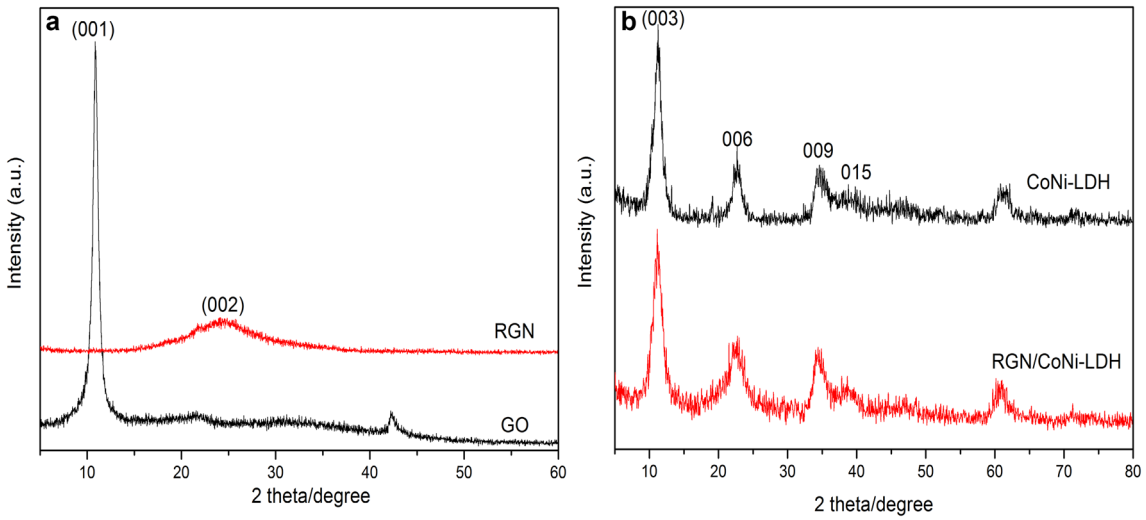

Fig. 4 XRD patterns of **a** GO, RGN, **b** CoNi-LDH and RGN/CoNi-LDH

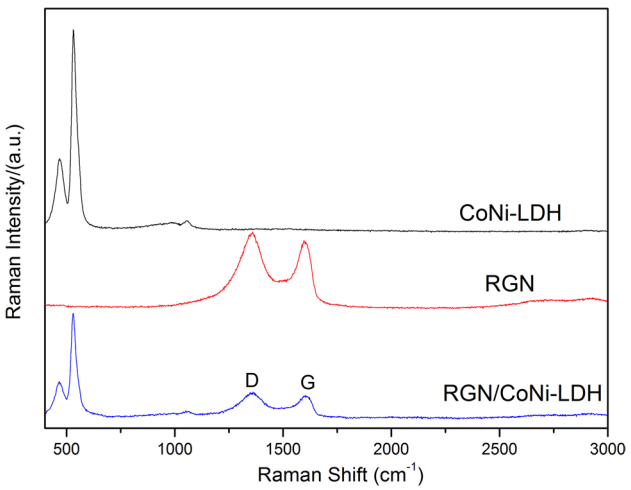

Fig. 5 Raman spectra of the RGN, CoNi-LDH, RGN/CoNi-LDH

This results effectively demonstrated CoNi-LDH composite have grown on the RGN nanosheets surface. For pure RGN, I_D/I_G value (1.074) is obtained. The I_D/I_G value (1.074) of RGN/CoNi-LDH composite (1.146) is further increased due to the incorporation of NiCo–LDH nanosheets, which would induce more defects and disorders of RGN [38].

XPS is employed to explore the chemical compositions and structure of CoNi-LDH and RGN/CoNi-LDH. Figure 6a, b show the change of atom of CoNi-LDH and RGN/CoNi-LDH. As shown in Fig. 6b, the survey spectrum indicates the presence of Co, Ni, C, N and O in the RGN/CoNi-LDH composite. The presence of C and N atoms illustrate that CoNi-LDH were successfully grown on RGN nanosheets. The deconvoluted Ni 2p and Co 2p peaks can be attributed to the formation of $Ni(OH)_2$ and $Co(OH)_2$ in CoNi-LDH and RGN/CoNi-LDH, respectively. Figure 6c shows the Ni 2p XPS spectrum, besides two shakeup satellites (indicated as ''Sat''), there are two major peaks at 855.77 and 873.21 eV, corresponding to Ni $2p_{3/2}$ and Ni $2p_{1/2}$, respectively. The spin-energy separation of 17.44 eV is characteristic of $Ni(OH)_2$ [39]. The Co 2p peak is further analyzed by high-resolution XPS (Fig. 6d). The Co 2p 3/2 and Co 2p 1/2 peaks of the $Co(OH)_2$ are at 781.27 and 796.8 eV with a 15.53 eV peak-to-peak separation, characteristic doublet of core-level Co 2p 3/2, 1/2, indicating the Co(II) oxidation state [40]. The C 1s XPS spectrum (Fig. 6e) can be deconvoluted into three different peaks centered at 284.65, 285.6, 287.4 and 288.7 eV, corresponding to C=C/C–C, C–N, C=O and O=C–O groups, respectively [41]. The N 1s XPS spectrum (Fig. 6f) can be deconvoluted into three different peaks centered at 398.7, 399.8 and 400.8 eV, corresponding to pyridine-N, pyrrole-N and quaternary-N [42]. Specifically, pyridinic-N and pyrrole-N are believed to provide pseudocapacitance through the redox reaction. The XPS survey spectra confirmed the formation of $Ni(OH)_2$ and $Co(OH)_2$ on the RGN surfaces.

3.2 Electrochemical performance of electrodes in NaOH electrolyte

Figure 7a presents the CV curves of CoNi-LDH and RGN/CoNi-LDH electrodes at a scan rate of 5 mV s^{-1}. A set of redox peak couples can be observed in the curves, demonstrating that the energy storage mechanism is based on the pseudocapacitance. The redox reaction take place as follows [43].

$$Ni(OH)_2 + OH^- \leftrightarrow NiOOH + H_2O + e^- \quad (4)$$

$$Co(OH)_2 + OH^- \leftrightarrow CoOOH + H_2O + e^- \quad (5)$$

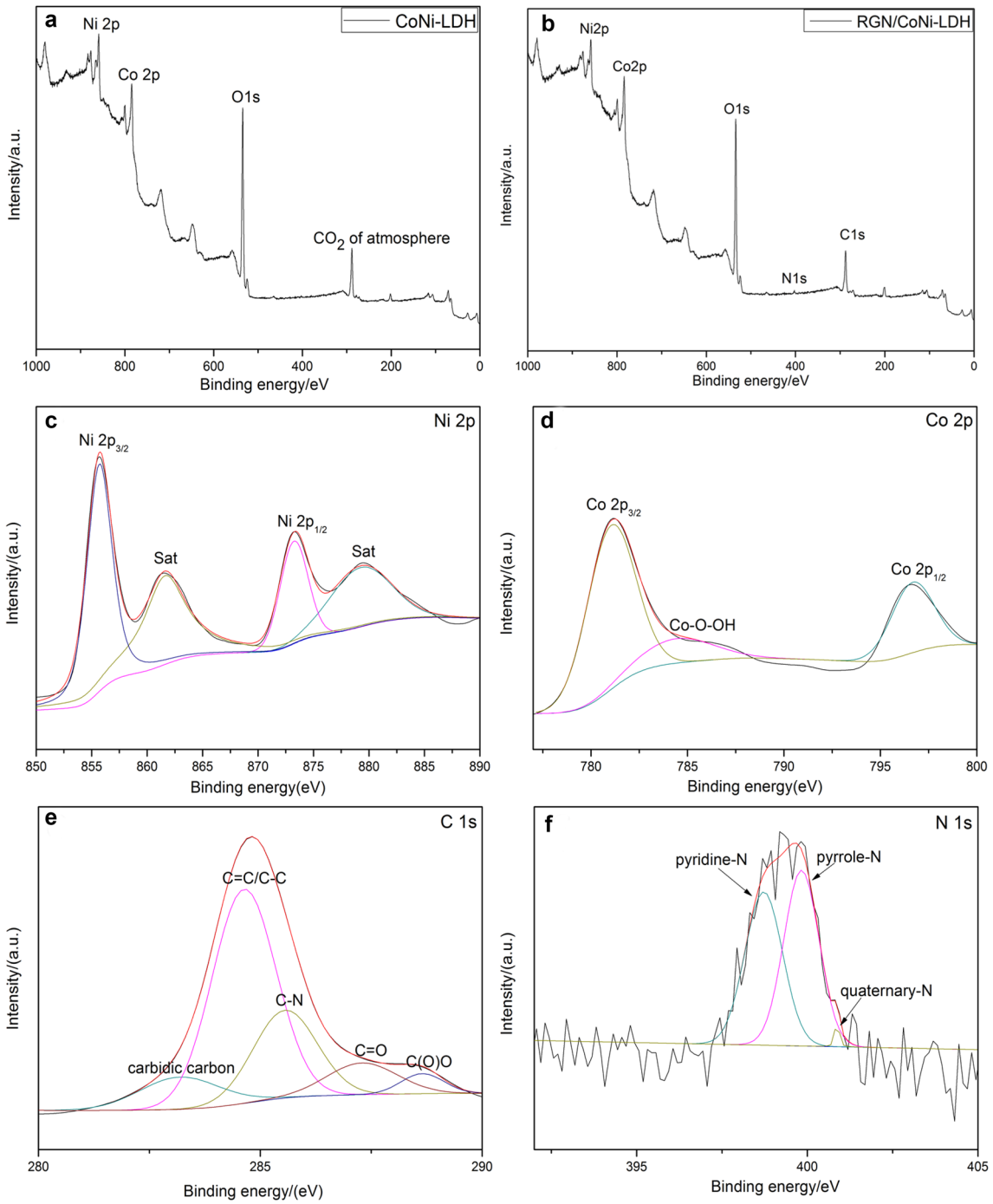

Fig. 6 **a** The XPS survey spectra of CoNi-LDH; **b** the XPS survey spectra of RGN/CoNi-LDH; **c** Ni 2p; **d** Co 2p; **e** C 1s; **f** N 1s

$$CoOOH + OH^- \leftrightarrow CoO_2 + H_2O + e^- \quad (6)$$

Individual oxidation and reduction peaks of nickel hydroxide and cobalt hydroxide cannot be observed, which is attributed to the similar oxidation and reduction behaviors of nickel hydroxide and cobalt hydroxide.

The CV curves at different scan rates of 3–20 mV s^{-1} for RGN/CoNi-LDH electrode are given in Fig. 7b. Apparently, with increasing scan rate and current density, the anodic peaks and cathodic peaks shift the more positive and negative direction. However, the figure of CV of RGN/CoNi-LDH remains unchanged clearly, which imply a high reversibility and good rate capability of RGN/CoNi-LDH electrode. The specific capacitance values were calculated from the discharge curves according to Eq. (1) and as shown in Fig. 7c. The discharge time of RGN/CoNi-LDH

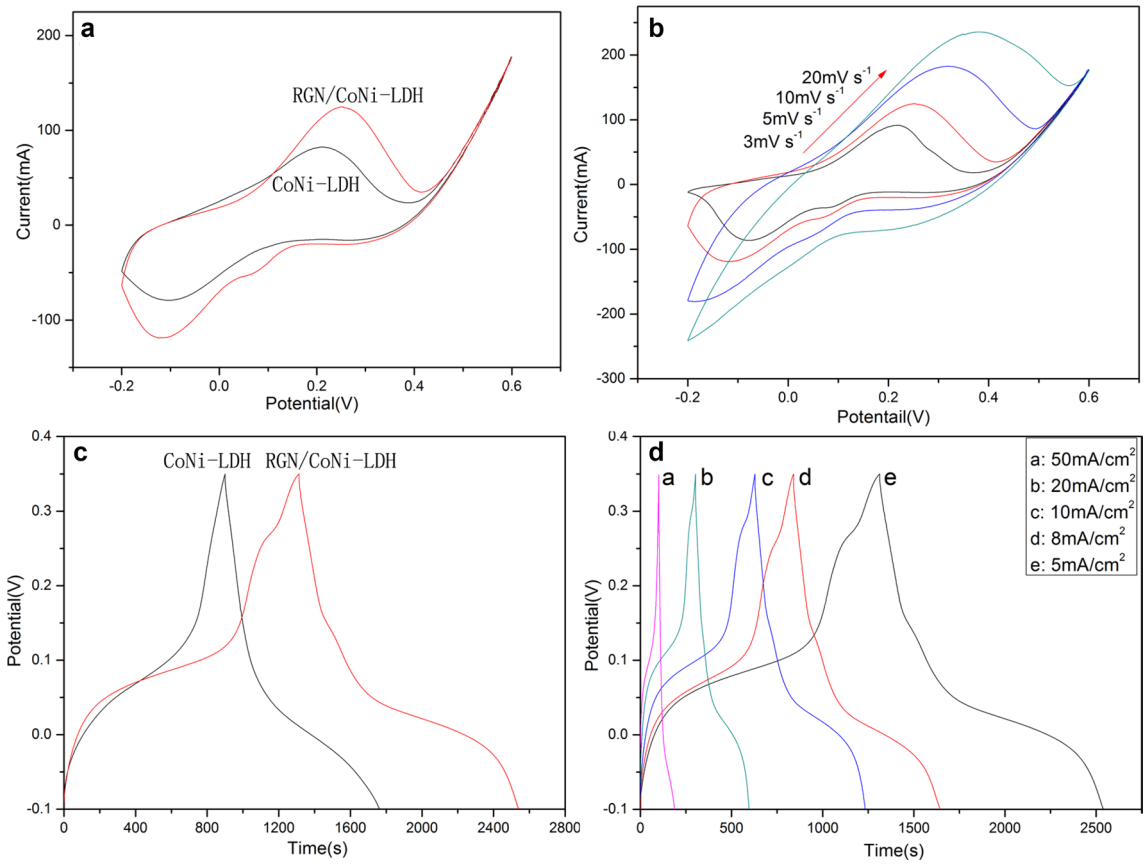

Fig. 7 **a** CV curves of the CoNi-LDH and RGN/CoNi-LDH samples at 5 mV s^{-1}. **b** CV curves of RGN/CoNi-LDH samples at different scan rates. **c** GCD curves of CoNi-LDH and RGN/CoNi-LDH samples at 5 mA cm^{-2}. **d** CP curves of RGN/CoNi-LDH samples at different current density

is longer than CoNi-LDH. The RGN/CoNi-LDH exhibits a specific capacitance value of 2092.3 F g^{-1} at the current density of 5 mA cm^{-2} compared to CoNi-LDH (1479 F g^{-1}). Figure 7d displays galvanostatic charge/discharge (GCD) curves of RGN/CoNi-LDH at various current densities of 5–50 mA cm^{-2}. The RGN/CoNi-LDH exhibits a specific capacitance value of 1810.86 F g^{-1} at the current density of 50 mA cm^{-2}. The rate retention of RGN/CoNi-LDH is 86.5% compared to CoNi-LDH of 76.5%. This should be attributed to nitrogen doping graphene can improve effectively electrical conductivity and the dispersion of CoNi-LDH and finally improve the specific capacitance and rate retention.

EIS was employed to further examine the charge-transfer and ion transport, electrochemical impedance spectroscopy. Figure 8 shows the Nyquist plots of the CoNi-LDH composites and RGN/CoNi-LDH electrodes. Two plots possess similar characteristic of semicircle in high and inclined line in the low frequency region. At high frequency region, the intersection of the semi-circle on the real axis represents the equivalent series resistance (Rs) of the electrode. Rs is the solution resistance in the circuit which represents the value

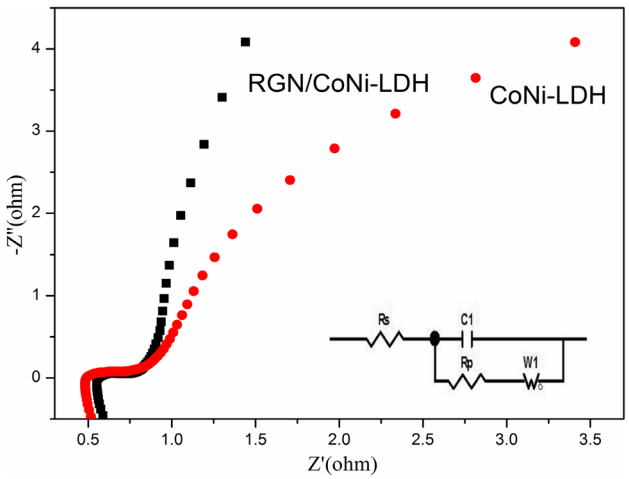

Fig. 8 Nyquist plots for CoNi-LDH and RGN/CoNi-LDH samples, the inset shows the equivalent circuit

of ohmic resistance of the electrolyte and the internal resistance of the electrode materials, the diameter of the semicircle represents the charge-transfer resistance (Rp) of the

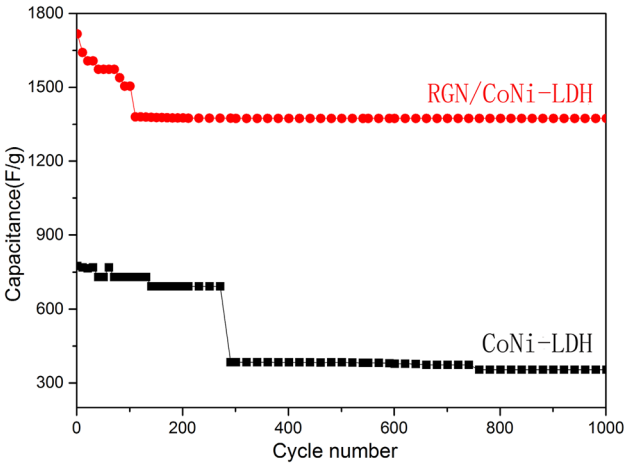

Fig. 9 Cycle performance for CoNi-LDH and RGN/CoNi-LDH samples at current density of 10 mA cm^{-2}

electrodes and electrolyte interface, the slope of the curve in the low-frequency region shows Warburg impedance (W), which represents electrolyte diffusion in the porous and proton diffusion in the host materials [44]. The intercepts of the Nyquist curves of CoNi-LDH and RGN/CoNi-LDH on the real axis are about 0.5–0.6 V, which indicate two kinds of electrode materials own low Rs. The diameter of the semicircle of RGN/CoNi-LDH is less than the diameter of the semicircle of CoNi-LDH, which represents the Rp of RGN/CoNi-LDH (0.223 Ω) is less than CoNi-LDH (0.377 Ω). The lower Rp of RGN/CoNi-LDH is attributes to the following facts: (i) RGN can effectively prevent the agglomeration of CoNi-LDH. (ii) RGN can greatly improve the electrical conductivity of CoNi-LDH, resulting higher capacitance retention. At low frequency region, the almost vertical line of RGN/CoNi-LDH represents the fast ion diffusion in electrolyte, which indicates the desired capacitive behavior.

From Fig. 9, the RGN/CoNi-LDH displays a better cyclic ability than CoNi-LDH at a current density of 10 mA cm^{-2}. The capacitance retention of RGN/CoNi-LDH of 80% is attained after 1000 cycle tests compared to CoNi-LDH of 50%. The well cycle ability of RGN/CoNi-LDH is attributed to the good mechanical properties and conductivity of RGN.

In order to test the energy density and power density of RGN/CoNi-LDH composite, an asymmetric supercapacitor (ASC) was assembled with RGN/CoNi-LDH as the positive electrode material, and active carbon (AC) as the negative electrode material, which is marked as RGN/CoNi-LDH//AC. The potential window of CV and GCD of the RGN/CoNi-LDH//AC is set as 1.53 V, which is attributed to the sum of the potential window for the RGN/CoNi-LDH and AC electrodes as shown in Fig. 10a. The mass ratio of RGN/CoNi-LDH and AC electrode is calculated as $m_+/m_- = 0.25$ according to following equation [43, 45]:

$$m_+/m_- = C_- \times \Delta V_-/(C_+ \times \Delta V_+) \quad (7)$$

The specific capacitance of AC and RGN/CoNi-LDH is 234.44 F g^{-1} and 2092.3 F g^{-1}, respectively, at current density of 5 mA cm^{-2} in 6 M KOH aqueous electrolyte solution. The potential window of AC and RGN/CoNi-LDH is 0.9 V and 0.45 V, respectively. The loading mass of AC and RGN/CoNi-LDH is 30 mg cm^{-2} and 7.5 mg cm^{-2}, respectively. The total mass of RGN/CoNi-LDH//AC is 37.5 mg cm^{-2}. Figure 10b shows the CV curves at different scan rates of 3–20 mV s^{-1} for RGN/CoNi-LDH//AC electrode. The asymmetric system shows a stable potential window of 1.53 V, and the non-rectangular curve shape can be attributed to the faradaic reaction from the positive electrode. As shown in the Fig. 10c, the specific capacitance of RGN/CoNi-LDH//AC is 151 F g^{-1} at the current density of 5 mA cm^{-2} according to the Eq. (1). The energy density of RGN/CoNi-LDH//AC is 49.4 Wh kg^{-1} at the power density of 101.97 W kg^{-1} according to the Eqs. (2) and (3). From Fig. 10d, RGN/CoNi-LDH//AC shows an excellent electrochemical stability with 88.8% of the initial capacity after 1000 cycles.

4 Conclusions

In summary, RGN/CoNi-LDH composites were fabricated by the co-precipitation method. These CoNi-LDH nanoflakes were grown on the surfaces of RGN in the hybrid. The presence of RGN can effectively improve the conductivity of composites and prevent the aggregation of CoNi-LDH, which promotes the electron and ions transfer of the active material. Electrochemical measurements indicated the capacitive performances of hybrid materials that could be improved by addition of RGN. RGN/CoNi-LDH composites had a high specific capacitance of 2092.3 F g^{-1} at current density of 5 mA cm^{-2} in 6 M KOH aqueous electrolyte solution and a good cycling stability. The rate retention of RGN/CoNi-LDH is 86.5% at current density of 5–50 mA cm^{-2}. An asymmetric capacitor was assembled with RGN/CoNi-LDH and activated carbon as positive and negative electrode, respectively. It had a high specific capacitance and an energy density.

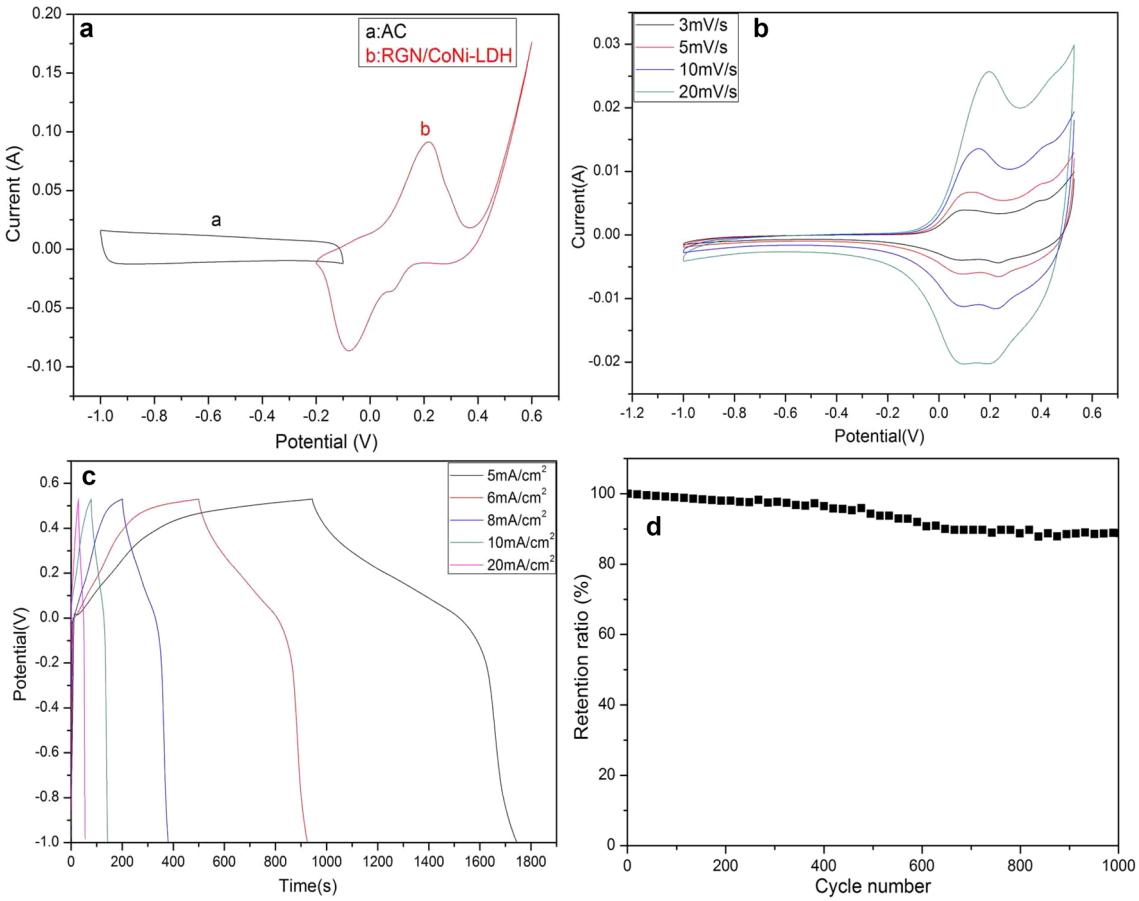

Fig. 10 **a** The CV curves of AC and RGN/CoNi-LDH single electrodes at a scan rate of 5 mV s^{-1}. **b** The CV curves of RGN/CoNi-LDH at different scan rates. **c** The GCD curves of RGN/CoNi-LDH at different current density. **d** Cycling stability of RGN/CoNi-LDH// AC device within the potential window of − 1 to 0.5 V at the current density of 10 mV s^{-1}

Acknowledgements This work was supported by the Gansu Provincial Education Department (2016A-148); National Natural Science Foundation of China (NSFC) (51503092, 51663014); Foundation of Key Laboratory of Clay Mineral Applied Research of Gansu Province, Lanzhou Institute of Chemical Physics, Chinese Academy of Sciences (CMAR-04); Foundation for Innovation Groups of Basic Research in Gansu Province (No. 1606RJIA322).

References

1. P. Simon, Y. Gogotsi, Materials for electrochemical capacitors. Nat. Mater. **7**, 845–854 (2008)
2. D.W. Wang, F. Li, M. Liu, G.Q. Lu, H.M. Cheng, 3D aperiodic hierarchical porous graphitic carbon material for high-rate electrochemical capacitive energy storage. Angew. Chem. **120**, 379–382 (2008)
3. J.Y. Wei, J.A. Zhang, Y. Liu, G.H. Xu, Z.M. Chen, Q. Xu, Controlled growth of whisker-like polyaniline on carbon nanofibers and their long cycle life for supercapacitors. RSC Adv. **3**, 3957–3962 (2013)
4. Y. Xu, Z. Lin, X. Huang, Y. Liu, Y. Huang, X. Duan, Flexible solid-state supercapacitors based on three-dimensional graphene hydrogel films. ACS Nano **7**, 4042–4049 (2013)
5. D. Usachov, O. Vilkov, A. Gruneis et al., Nitrogen-doped graphene: efficient growth, structure, and electronic properties. Nano Lett. **11**, 5401–5407 (2011)
6. G.H. Jun, S.H. Jin, B. Lee et al., Enhanced conduction and charge-selectivity by N doped graphene flakes in the active layer of bulk-heterojunction organic solar cells. Energy Environ. Sci. **6**, 3000–3006 (2013)
7. A. Sliwak, B. Grzyb, N. Díez, G. Gryglewicz, Nitrogen-doped reduced graphene oxide as electrode material for high rate supercapacitors. Appl. Surf. Sci. **399**, 265–271 (2017)
8. J. Li, Z. Ren, Y. Zhou et al., Scalable synthesis of pyrrolic N-doped graphene by atmospheric pressure chemical vapor deposition and its terahertz response. Carbon **62**, 330–336 (2013)
9. I.Y. Jeon, H.J. Choi, M.J. Ju et al., Direct nitrogen fixation at the edges of graphene nanoplatelets as efficient electrocatalysts for energy conversion. Sci. Rep. **3**, 2260–2266 (2013)
10. N. Li, Z.Y. Wang, K.K. Zhao et al., Large scale synthesis of N-doped multi-layered graphene sheets by simple arc-discharge method. Carbon **48**, 255–259 (2010)

11. P. Simon, Y. Gogotsi, Charge storage mechanism in nanoporous carbons and its consequence for electrical double layer capacitors. Philos. Trans. R. Soc. A **368**, 3457–3467 (2010)
12. C. Wang, J. Xu, M.F. Yuen et al., Hierarchical composite electrodes of nickel oxide nanoflake 3D graphene for high-performance pseudocapacitors. Adv. Funct. Mater. **24**, 6372–6380 (2014)
13. H. Wang, H.S. Casalongue, Y.D. Liang, $Ni(OH)_2$ nanoplates grown on grapheme as advanced electrochemical pseudocapacitor materials. J. Am. Chem. Soc. **132**(21), 7472–7477 (2010)
14. R. Kumar, H.J. Kim, S. Park, A. Sricastava, I.K. Oh, Graphene-wrapped and cobalt oxide-intercalated hybrid for extremely durable super-capacitor with ultrahigh energy and power densities. Carbon **79**, 192–202 (2014)
15. Z.C. Huang, S.L. Wang, J.P. Wang, Y.M. Yu, J. Wen, R. Li, Exfoliation-restacking synthesis of coal-layered double hydroxide nanosheets/reduced graphene oxide composite for high performance supercapacitors. Electrochim. Acta **152**, 117–125 (2015)
16. G.X. Pan, X.H. Xia, J.S. Luo et al., Preparation of CoAl layered double hydroxide nanoflake arrays and their high supercapacitance performance. Appl. Clay Sci. **102**, 28–32 (2014)
17. J. Wang, Y.C. Song, Z.S. Li, Q. Liu, J.D. Zhou, X.Y. Jing, M.L. Zhang, Z.H. Jiang, In situ Ni/Al layered double hydroxide and its electrochemical capacitance performance. Energy Fuels **24**, 6463–6467 (2010)
18. X. Wang, A. Sumboja, M. Lin, J. Yan, P.S. Lee, Enhancing electrochemical reaction sites in nickel-cobalt layered double hydroxides on zinc tin oxide nanowires: a hybrid material for an asymmetric supercapacitor device. Nanoscale **4**, 7266–7272 (2012)
19. X. Sun, G. Wang, H. Sun, F. Lu, M. Yu, J. Lian, Morphology controlled high performance supercapacitor behaviour of the Ni–Co binary hydroxide system. J. Power Sources **238**, 150–156 (2013)
20. J. Yang, C. Yu, X.M. Fan, Z. Ling, J.S. Qiu, Y. Gogotsi, Facile fabrication of MWCNT-doped NiCoAl-layered double hydroxide nanosheets with enhanced electrochemical performances, J. Mater. Chem. A **1**, 1963–1968 (2013)
21. M. Jana et al., Growth of Ni–Co binary hydroxide on a reduced graphene oxide surface by a successive ionic layer adsorption and reaction (SILAR) method for high performance asymmetric supercapacitor electrodes. J. Mater. Chem. A **4**, 2188–2197 (2016)
22. H. Chen, L. Hu, M. Chen, Y. Yan, L. Wu, Nickel–cobalt layered double hydroxide nanosheets for high-performance supercapacitor electrode materials. Adv. Funct. Mater. **24**, 934–942 (2014)
23. S.N. Tiruneh, B.K. Kang, Q.T. Ngoc, D.H. Yoon, Enhanced electrochemical performance of lamellar structured Co–$Ni(OH)_2$ /reduced graphene oxide (rGO) via hydrothermal synthesis. RSC Adv. **6**, 4764–4769 (2016)
24. H. Xu, J. Liu, Y. Chen, C.L. Li, J. Tang, Q. Li, Synthesis of three-dimensional nitrogen-doped graphene/polyaniline hydrogels for high performance supercapacitor applications. J. Mater. Sci.: Mater. Electron. **28**, 10674–10683 (2017)
25. L. Qiu, J.Z. Liu, S.L.Y. Chang, Y. Wu, D. Li, Biomimetic superelastic graphene-based cellular monoliths. Nat. Commun. **3**, 1241–1247 (2012)
26. Z.A. Hu, Y.L. Xie, Y.M. Wang, H.Y. Wu, Y.Y. Yang, Z.Y. Zhang, Synthesis and electrochemical characterization of mesoporous Co_xNi_{1-x} layered double hydroxides as electrode materials for supercapacitors. Electrochim. Acta **54**, 2737–2741 (2009)
27. W.J. Wang, Q.L. Hao et al., Ternary nitrogen-doped graphene/nickel ferrite/polyaniline nanocomposites for high-performance supercapacitors. J. Power Sources **269**, 250–259 (2014)
28. M. Li, J.P. Cheng, J. Wang et al., The growth of nickel-manganese and cobalt-manganese layered double hydroxides on reduced graphene oxide for supercapacitor. Electrochim. Acta **206**, 108–115 (2016)
29. H. Jeong, Y. Pyo Lee, M. Hua Jin et al., Thermal stability of graphite oxide. Chem. Phys. Lett. **470**, 255–258 (2009)
30. J. Zhang, H. Yang, G. Shen, P. Cheng, J. Zhang et al., Reduction of graphene oxide via L-ascorbic acid. Chem. Commun. **46**, 1112–1114 (2010)
31. B. Wang, Q. Liu, Z. Qian, X. Zhang, J. Wang, Z. Li, H. Yan, Z. Gao, F. Zhao, L. Liu, Two steps in situ structure fabrication of Ni–Al layered double hydroxide on Ni foam and its electrochemical performance for supercapacitors. J. Power Sources **246**, 747–753 (2014)
32. J.P. Cheng, L. Liu, J. Zhang, F. Liu, X.B. Zhang, Influences of anion exchange and phase transformation on the supercapacitive properties of α-$Co(OH)_2$, J. Electroanal. Chem. **722–723**(3) 23–31 (2014)
33. J. Xu, S. Gai, F. He, N. Niu, P. Gao, Y. Chen, P. Yang, A sandwich-type three-dimensional layered double hydroxide nanosheet array/graphene composite: fabrication and high supercapacitor performance. J. Mater. Chem. A **2**, 1022–1031 (2014)
34. Z. Wang, X. Zhang, J.H. Wang, L.D. Zou, Z.T. Liu, Z.P. Hao, Preparation and capacitance properties of graphene/NiAl layered double-hydroxide nanocomposite. J. Colloid Interface Sci. **396**, 251–257 (2013)
35. J.C. Huang, T. Lei, X.P. Wei, X.W. Liu, T. Liu, D.X. Cao, J.L. Yin, G.L. Wang, Effect of Al-doped β-$Ni(OH)_2$ nanosheets on electrochemical behaviors for high performance supercapacitor application. J. Power Sources **232**, 370–375 (2013)
36. B. Guo, Q. Liu, E. chen, H. Zhu, L. Fang, J. Gong, Controllable N-doping of graphene. Nano Lett. **10**, 4975–4980 (2010)
37. J. Memon, J.H. Sun, D.L. Meng, W.Z. Ouyang, M.A. Memon, Y. Huang, S. Yan, J.X. Geng, Synthesis of graphene/Ni–Al layered double hydroxide nanowires and their application as an electrode material for supercapacitors. J. Mater. Chem. A **2**, 5060–5067 (2014)
38. Z.Y. Ji, X.P. Shen, J.L. Yang, G.X. Zhu, K.M. Chen, A novel reduced graphene oxide/Ag/CeO_2 ternary nanocomposite: Green synthesis and catalytic properties. Appl. Catal. B **144**, 454–461 (2014)
39. H. Wang, X. Xiang, F. Li, Facile synthesis and novel electrocatalytic performance of nanostructured Ni–Al layered double hydroxide/carbon nanotube composites. J. Mater. Chem. **20**, 3944–3952 (2010)
40. J.F. Moulder, W.F. Sticlke, P.E. Sobol, K.D. Bomben, in *Handbook of X-ray Photoelectron Spectroscopy*, ed. by J. Chastain (PerkinElmer Corporation, Eden Prairie, 1992)
41. S. Biniak, G. Szymaski, J. Siedlewski, A. Swiatkowski, The characterization of activited carbons with oxyger and nitrogen surface groups. Carbon **35**, 1799–1810 (1997)
42. J. Casanovas, J.M. Ricart, J. Rubio, F. Illas, J.M. Jimenez-Mateos, Origin of the large N 1s binding energy in X-ray photoelectron spectra of calcined carbonaceous materials. J. Am. Chem. Soc. **118**, 8071–8076 (1996)
43. V. Gupta, S. Gupta, N. Miura, Electrochemically synthesized large area network of Co_xNi_y alzlayered triple hydroxides nanosheets: a high performance supercapacitor. J. Power Sources **189**, 1292–1295 (2009)
44. J. Balamurugan, T.D. Thanh, S.B. Heo, N.H. Kim, J.H. Lee, Novel route to synthesis of N-doped graphene/Cu–Ni oxide composite for high electrochemical performance. Carbon **94**, 962–970 (2015)
45. X.Y. Meng, M.G. Feng, H. Zhang, Zh.G. Ma, C.M. Zhang, Solvothermal synthesis of cobalt/nickel layered double hydroxides for energy storage devices. J. Alloys Compd. **695**, 3522–3529 (2017)